Supplemental Material

Are the impacts of land use on warming underestimated in climate policy?

Calculation of radiative forcing

The computation of the LULCC and non-LULCC radiative forcings (RFs) used in this study, carried out by Ward et al. (2014), follows a three-step process. First, emissions of radiatively relevant trace gas and aerosol species are collected and partitioned into LULCC and non-LULCC categories, followed by determination of the change in atmospheric concentrations of these species through modeling, and culminating in calculation of the modified radiative transfer from these concentration changes. Ward et al. (2014) computed RF from LULCC and non-LULCC for CO_2, N_2O, CH_4, tropospheric O_3, aerosol direct and indirect effects, and land surface albedo changes. Here we describe the methods used for these computations with an emphasis on the LULCC RFs. Non-LULCC RFs were calculated using the same methods using emissions from fossil fuel burning and other industrial processes (Ward et al, 2014).

The partitioning of emissions into either LULCC or non-LULCC is standard for many trace gas species as part of bottom-up development of emission inventories, including CH_4, non-methane hydrocarbons (NHMCs), and black carbon and organic carbon aerosols (Lamarque et al., 2010). However, this is not the case for CO_2 or N_2O emissions, and existing inventories do not take into account changes in fire activity associated with LULCC.

Ward et al. (2014) computed the CO_2 flux from deforestation and LULCC-caused changes in fire activity for 1850 to 2100 by comparing the terrestrial C storage in a simulation using the Community Land Model version 3.5 (CLM; Oleson et al., 2008; Thornton et al., 2009) that included land cover conversions applied, to a simulation without land cover conversions. The CO_2 flux values were adjusted downward to correct for the CO_2-fertilization feedback, which is not represented in standalone terrestrial model simulations and leads to double-counting of CO_2 emissions (Arora and Boer, 2010). Global models produce a large range in estimates of historical CO_2 emissions from LULCC (Brovkin et al., 2013), largely due to uncertainty in terrestrial C storage but also resulting in part from terminology differences (Pongratz et al., 2014). The Ward et al. (2014) LULCC CO_2 flux estimate for the historical time period lies in the middle of this range. Atmospheric CO_2 concentrations were determined by Ward et al. (2014) using a pulse response function approach that prescribes the airborne fraction of emitted CO_2 for centuries after the initial emission (similar to the methodology used by Randerson et al., 2006; O'Halloran et al., 2012). Because CO_2 is a well-mixed greenhouse gas, these calculations were done on a global basis with no spatial distribution of emissions taken into account. Additional changes to the CO2 concentration due to the feedback of LULCC-driven changes in climate onto the carbon cycle (Mahowald, 2011) were also considered. The RF of the change in CO_2 concentration from the LULCC CO2 emissions was computed following Ramaswamy et al. (2001).

Agricultural activities dominate the anthropogenic production of N_2O while there are substantial emissions from natural processes in the soil and also a small amount emitted by wildfires (Kroeze et al., 1999). Ward et al. (2014) estimated future N_2O emissions from LULCC by scaling present day and historical emissions to projected cropland and pasture area. This assumes that agricultural fertilizer application practices remain similar during the next century. Changes in N_2O concentration in response to LULCC emissions can be calculated with a simple box-model approach assuming a known N_2O tropospheric lifetime. Ward et al. (2014) used the box-model described by Kroeze et al. (1999) and an adaptable N_2O lifetime following Meinshausen et al. (2011). The RF that results from the LULCC-driven changes in N_2O concentration was calculated using the expression given by Ramaswamy et al. (2001).

Ward et al. (2014) used available historical and projected emissions of CH_4 from LULCC activities that were produced for model intercomparison projects (Lamarque et al., 2010; van Vuuren et al., 2007; Wise et al., 2009; Fujino et al., 2006; Riahi et al., 2007) to compute the CH_4 RF for the LULCC and non-LULCC categories. A box-model was used by Ward et al. (2014) to compute changes in CH_4 concentration due to these emissions. However, CH_4 concentrations are also modified indirectly by changes to the oxidative capacity of the atmosphere, which affect the CH_4 lifetime. Ward et al. (2014) calculated the impact of LULCC on the CH_4 lifetime by simulating atmospheric chemistry within the Community Atmosphere Model version 4 (CAM4; Emmons et al., 2010; Hurrell et al., 2013) for scenarios with and without emissions of NHMCs and other trace gases from LULCC. The modeled changes in global hydroxyl radical concentrations caused by the LULCC emissions were then used to compute a new scenario-specific lifetimes for CH_4. The CH_4 concentrations were then re-calculated with the new lifetimes and the RF computed from the expression recommended in Ramaswamy et al. (2001).

The set of CAM4 simulations with and without LULCC emissions were also used to calculate changes in tropospheric O_3 due to LULCC (Ward et al., 2014). LULCC activities can impact O_3 concentrations through emission of NO_x from fertilizer use, and by modifying the landscape, which leads to changes in biogenic and fire emissions of NMHCs. O_3 lifetimes in the troposphere are too short for the forcing agent to be considered well-mixed spatially so box-model methods could not be applied here. Instead, the shortwave and longwave radiative impacts of the O_3 were calculated with global-scale offline radiative transfer code (Conley et al., 2013). Ward et al. (2014) also included consideration of the primary mode response of O_3 concentration to LULCC-driven changes in CH_4 (Prather et al., 2001).

Ward et al. (2014) include three ways in which LULCC can cause changes in aerosol emissions. Agriculture can lead to increased soil erosion by wind thereby enhancing dust emissions, and the expansion of agricultural land changes both the emission of biogenic aerosol precursor gases from natural vegetation, and emission of carbonaceous aerosols and sulfate from wildfires. A set of 5-year simulations with CAM version 5 (CAM5; Hurrell et al., 2013) combined with the 3-mode Modal Aerosol Model (MAM3; Liu et al., 2012) were run with and without the aerosol emissions from LULCC. Online radiative transfer diagnostics (Ghan et al., 2013) were used to compute the effective radiative forcing of the direct and indirect effects of the change in aerosol emissions. In addition, the forcing from aerosol deposition onto ice and snow surfaces, which causes an albedo change, was calculated online within these simulations using the SNICAR model (Flanner et al., 2007). This effect is particularly important for carbonaceous aerosols, but changes in mineral dust emissions due to LULCC also contribute to the RF. Finally, the biogeochemical feedbacks of aerosols onto CO2 concentrations that were quantified by Mahowald (2011) were included for LULCC-driven aerosol emission changes (Ward et al., 2014).

Finally, the albedo of the land surface itself can be modified by land cover conversions and wood harvesting. Land surface albedo change is simulated by CLM. Ward et al. (2014) use the output of land surface albedo change from the year 1850 to 2100 CLM simulations for different LULCC scenarios and a present day climatology of cloud cover and aerosol optical depth to determine the impact of the albedo change on atmospheric radiative fluxes. Albedo changes from LULCC-driven change in wildfire activity was also included in the total RF. The fire albedo change RF was computed following the methods of Ward et al. (2012).

Bibliography

Arora, V. K., Boer, G. J., 2010. Uncertainties in the 20th century carbon budget associated with land use change. Global Change Biology. 16**,** 3327-3348.

Brovkin, V., et al., 2013. Effect of anthropogenic land-use and land-cover changes on climate and land carbon storage in CMIP5 projections for the twenty-first century. Journal of Climate. 26**,** 6859-6881; doi:10.1175/JCLI-D-12-00623.1.

Conley, A., et al., 2013. PORT, a CESM tool for the diagnosis of radiative forcing. Geosci. Model Dev. 6**,** 469-476.

Flanner, M. G., et al., 2007. Present day climate forcing and response from black carbon in snow. J. Geophysical Research. 112**,** doi:1029/2006JD00803.

Fujino, J., et al., 2006. Multi-gas mitigation analysis on stabilzation scenarios using AIM global model. The Energy Journal Special Issue. 3**,** 343–354.

Ghan, S., 2013. Technical note: estimating aerosol effects on cloud radiative forcing. Atmospheric Chemistry and Physics. 13**,** 9971-9974.

Hurrell, J. W., et al., 2013. The Community Earth System Model: A Framework for Collaborative Research. Bulletin of the American Meteorological Society. 0.1175/BAMS-D-12-00121.

Kroeze, C., et al., 1999. Closing the global

N2O budget: A retrospective analysis 1500–199. Global Biogeochemical Cycles. 13**,** 1-8.

Lamarque, J.-F., et al., 2010. Historical (1850-200) gridded anthropogenic and biomass burning emissions of reactive gases and aerosols: methodology and application. Atmospheric Chemistry and Physics. 10**,** 7017-7039.

Liu, X., et al., 2011. Toward a minimal representation of aerosol direct and indirect ef fects: model description and evaluation. Geoscientific Model Development Discussions. 4**,** 3485-3598.

Mahowald, N., 2011. Aerosol indirect effect on biogeochemistry and climate. Science. 334**,** 794-796.

Meinshausen, M., et al., 2011. The RCP greenhouse gas concentrations and their extensions from 1765 to 2300. Climatic Change. soi:10.1007/s10584-011-0156-z.

O'Halloarn, T., et al., 2012. Radiative forcing of natural forest disturbances. Global Change Biology. 18**,** 555-565.

Oleson, K. W., et al., 2008. Improvements to the Community Land Model and their impact on the hydrological cycle. Journal of Geophysical Research. 113**,** doi:10.1029/2007JG000563.

Pongratz, J., et al., 2014. Terminology as a key uncertainty in net land use and land cover change carbon flux estimates. Earth System Dynamics. 5**,** 177-195.

Prather, M., et al., Atmospheric Chemistry and Greenhouse Gases. In: J. T. Houghton, Ding, Y., Griggs, D. J., Noguer, M., Van der Linden, P. J., Dai, X., Maskell, K., and Johnson, C. A., (Ed.), Climate Change 2001: The Scientific Basis. Cambridge University Press, Cambridge, UK, 2001.

Ramaswamy, V., al., e., Radiative forcing of climate changeim. In: J. e. a. Houghton, (Ed.), Climate Change 2001: The Scientific Basis. Contribution of Working Group I to the Third Assessment Report of the Intergovernmental Panel on Climate Change. Cambridge University Press, Cambridge, UK, 2001.

Randerson, J., et al., 2006. The impact of boreal forest fire on climate warming. Science. 314**,** 1130-1132.

Riahl, K., et al., 2007. Scenarios of long-term socio-economic and environmental development under climate stabilization. Technological Forecasting and Social Change. 74**,** 887-935.

Thornton, P., et al., 2009. Carbon-nitrogen interactions regular climate-carbon cycle feedbacks: results from an atmosphere-ocean general circulation model. Biogeosciences. 6**,** 2099-2120; doi:10.5194/bg-5-2099-2009.

van Vuuren, D. P., et al., 2011. The representative concentration pathways: an overview. Climatic Change. 109**,** 5-31.

Ward, D., et al., 2012. The changing radiative forcing of fires: Global model estimates for past, present and future. Atmospheric Chemistry and Physics. http://www.atmos-chem-phys-discuss.net/12/10535/2012/acpd-12-10535-2012.html.
Ward, D. S., Mahowald, N., 2014. Contributions of developed and developing countries to global climate forcing. Environmental Research Letters. 9**,** doi:10.1088/1748-9326/9/7/074008.
Wise, M., et al., 2009. Implications of limiting CO2 concentrations for land use and energy. Science. 324**,** 1183-1186.

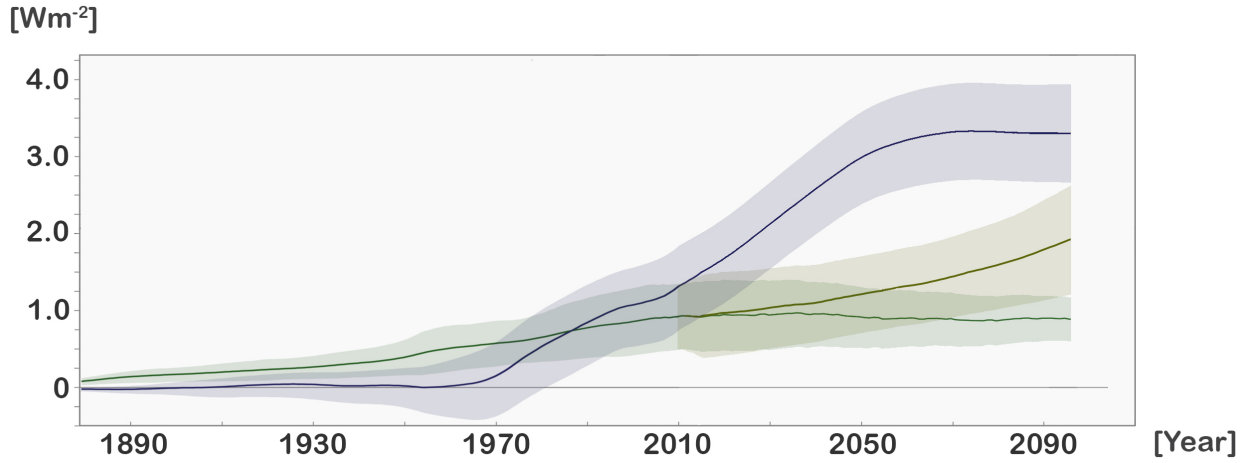

Figure S1: Decadal average net anthropogenic radiative forcing relative to 1850 from the LULCC (green - historical and RCP4.5; brown – TBAU) and non-LULCC (blue) scenarios used to determine the temperature in panel a. The radiative forcing terms are calculated in (Ward and Mahowald, 2015; Ward et al., 2014) for LULCC and other sources (labeled non-LULCC here). The shaded region surrounding each timeseries represents the uncertainty in the partitioning of the RF between the LULCC and non-LULCC sectors.

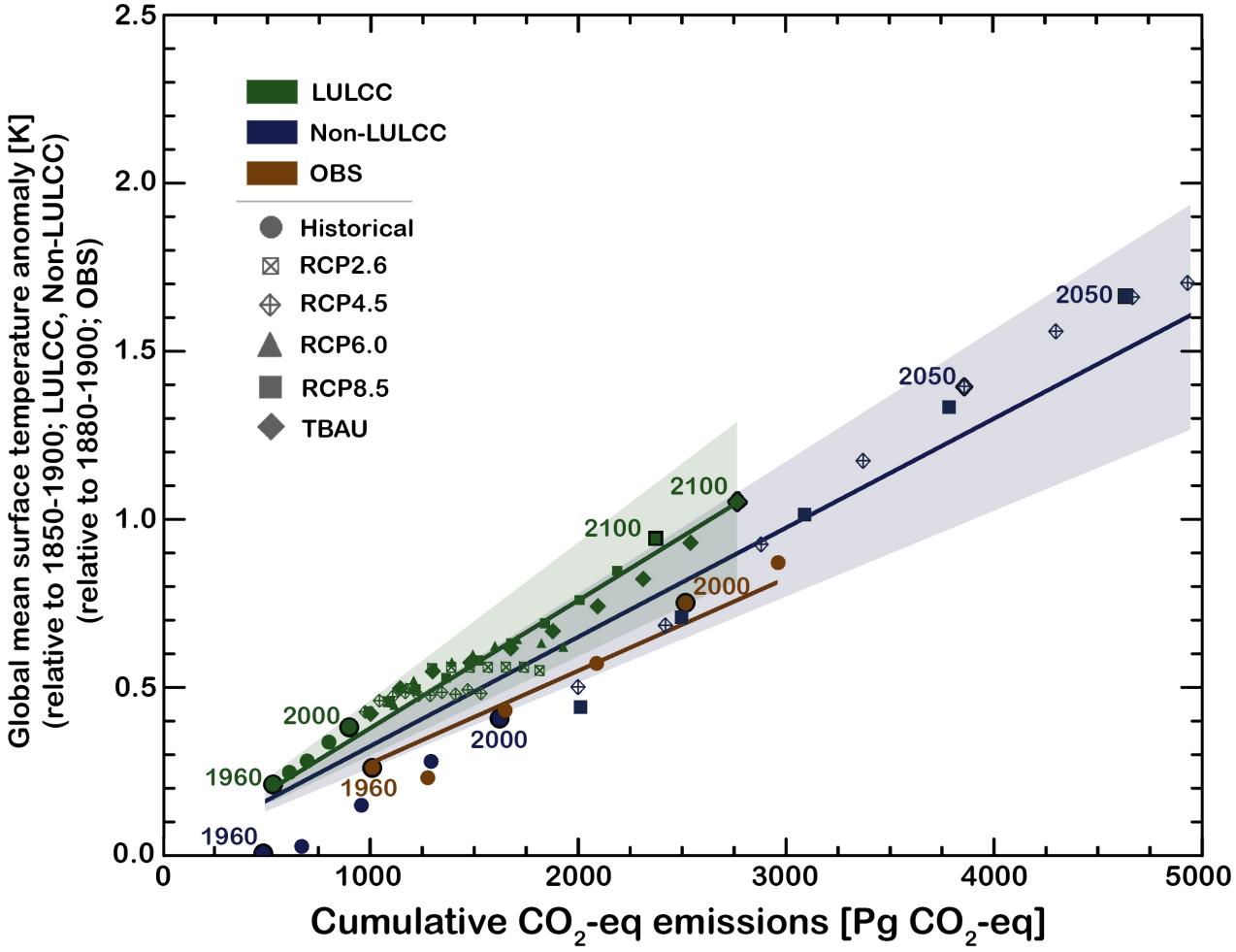

Figure S2: Change in global mean surface temperature relative to the 1850-1900 mean for cumulative carbon dioxide equivalent (CO_2-eq) emissions from different LULCC and non-LULCC scenarios. This figure is the same as Figure 2 in the text, except that here cumulative CO_2-eq is used instead of CO_2. Here, CO_2-equivalents are calculated using global warming potentials for CO_2, CH_4, N_2O and halocarbon species from the IPCC AR5 (Myhre et al., 2013) and a 100 year time horizon. The temperature increase associated with the cumulative CO_2-eq emissions (but including other emissions and forcings) is plotted for every ten years in the 1850-2100 time series with historical points (circles), RCP2.6 (x's), RCP4.5 (crosses), RCP6.0 (triangles), RCP8.5 (squares) and tropical business as usual (TBAU) (diamonds) for land use and land cover change (LULCC), shown in green. The temperature increase for other sources of anthropogenic forcing (labeled non-LULCC) in blue using RCP4.5 (crosses), and RCP8.5 (squares). The radiative forcings are calculated in (Ward and Mahowald, 2015; Ward et al., 2014) for LULCC versus other sources (non-LULCC). The observed temperature is shown in brown using GISS temperature observations and estimated cumulative emissions. The interquartile range is determined from the MAGICC6 simulation ensemble and the regression lines are fit to yearly values for all historical and future scenario points between 1960 and 2100.